Arctic Stratus Cloud Properties and Radiative Forcing Derived from Ground-Based Data Collected at Barrow, Alaska

XIQUAN DONG* AND GERALD G. MACE

University of Utah, Salt Lake City, Utah

(Manuscript received 21 June 2001, in final form 13 August 2002)

ABSTRACT

A record of single-layer and overcast low-level Arctic stratus cloud properties has been generated using data collected from May to September 2000 at the Atmospheric Radiation Measurement (ARM) North Slope of Alaska (NSA) (71.3°N, 156.6°W) site near Barrow, Alaska. The record includes liquid-phase and liquid dominant mixed-phase Arctic stratus macrophysical, microphysical, and radiative properties, as well as surface radiation budget and cloud radiative forcing. The macrophysical properties consist of cloud fractions, cloud-base/top heights and temperatures, and cloud thickness derived from a ground-based radar and lidar pair, and rawinsonde sounding. The microphysical properties include cloud liquid water path and content, and cloud-droplet effective radius and number concentration obtained from microwave radiometer brightness temperature measurements, and the new cloud parameterization. The radiative properties contain cloud optical depth, effective solar transmission, and surface/cloud/top-of-atmosphere albedos derived from the new cloud parameterization and standard Epply precision spectral pyranometers. The shortwave, longwave, and net cloud radiative forcings at the surface are inferred from measurements by standard Epply precision spectral pyranometers and pyrgeometers. There are approximately 300 h and more than 3600 samples (5-min resolution) of single-layer and overcast low-level stratus during the study period. The 10-day averaged total and low-level cloud ($Z_{top} < 3$ km) fractions are 0.87 and 0.55, and low-level cloud-base and -top heights are around 0.4 and 0.8 km. The cloud-droplet effective radii and number concentrations in the spring are similar to midlatitude continental stratus cloud microphysical properties, and in the summer they are similar to midlatitude marine stratus clouds. The total cloud fractions in this study show good agreement with the satellite and surface results compiled from data collected during the First International Satellite Cloud Climatology Project (ISCCP) Regional Experiment (FIRE) Arctic Cloud Experiment (ACE) and the Surface Heat Budget of the Arctic Ocean (SHEBA) (~77°N, 165°W) field experiments in 1998. The cloud microphysics derived from this study are similar, in general, to those collected in past field programs, although these comparisons are based on data collected at different locations and years. At the ARM NSA site, the summer cooling period is much longer (2–3 months vs 1–2 weeks), and the summer cooling magnitude is much larger (-100 W m^{-2} vs -5 W m^{-2}) than at the SHEBA ship under the conditions of all skies at the SHEBA and overcast low-level stratus clouds at the NSA site.

1. Introduction

Clouds are the dominant modulators of radiation in the Arctic both at the surface and top of atmosphere. Their impact on the radiation fluxes depends on cloud particle size and shape, and the amount and phase of condensed water and its vertical and horizontal distributions (Curry et al. 2000; Randall et al. 1998). The cloud–radiative interactions in the Arctic are very complex due to low temperatures and absolute humidity, large solar zenith angles, the presence of the highly reflective and inhomogeneous snow/ice surfaces and multiple cloud layers, and persistent temperature inversions (Curry et al. 1996; Stamnes et al. 1999). The importance of cloud–radiative interactions to global climate has been highlighted by many investigators (e.g., Wetherald and Manabe 1988; Mitchell and Ingram 1992) and recent climate modeling results have revealed that the largest disagreement between coupled climate model simulations of present-day climate is found in the Arctic region (Gates 1992; Tao et al. 1996). These results reflect the weakness of our current understanding of the sensitivity of the simulated Arctic climate to different formulations of various physical processes in global models (Randall et al. 1998). An aspect of Arctic clouds that makes them difficult to treat in climate models is that they are often optically thin, so that their emissivities are often less than one and a function of particle size (Garrett et al. 2002; Curry and Ebert 1992). The albedo of snow has a strong spectral variation and is a function of the ratio of direct-to-diffuse radiation,

*Current affiliation: Department of Atmospheric Sciences, University of North Dakota, Grand Forks, North Dakota.

Corresponding author address: Dr. Xiquan Dong, Department of Atmospheric Sciences, University of North Dakota, Box 9006, Grand Forks, ND 58202-9006.
E-mail: dong@aero.und.edu

both of which are affected by cloud optical depth, which further complicates the treatment of radiative transfer in the cloudy Arctic (Curry et al. 2001).

To provide a much-needed source of high-latitude data concerning the physical state of the Arctic atmosphere, several extensive field programs have been conducted in the past several years. The Department of Energy Atmospheric Radiation Measurement (ARM) program (Stokes and Schwartz 1994) established the ARM North Slope of Alaska (NSA) site (71.3°N, 156.6°W) at Barrow, Alaska, in 1998 (Stamnes et al. 1999). The general approach adopted by the ARM program is to use long records of surface observations to develop, test, and improve cloud parameterizations in the context of single GCM grid columns and then to transfer the resulting parameterizations into full three-dimensional GCMs (Randall et al. 1996). As a precursor to the establishment of the site at Barrow, the ARM program operated concurrently with the First International Satellite Cloud Climatology Project (ISCCP) Regional Experiment (FIRE) Arctic Cloud Experiment (ACE; Curry et al. 2000) and the Surface Heat Budget of the Arctic Ocean (SHEBA) project (Perovich et al. 1999). In addition to observations collected at Barrow, ARM surface-based instruments were also installed on or near the SHEBA ship that served as a floating science station in the Beaufort Sea and drifted from 75.3°N, 142.7°W to 80.5°N, 166°W during October 1997–October 1998. FIRE ACE made aircraft observations and satellite retrievals over the SHEBA ship (at ~77°N, 165°W) and Barrow from April to July 1998 (Curry et al. 2000). ARM, FIRE, and SHEBA share scientific objectives that focus on collecting and evaluating data so that the physical processes that drive the large-scale atmosphere in the Arctic are more faithfully represented (Randall et al. 1998). In particular, ARM has a long-term program (~10 yr) of surface-based observations and modeling of clouds and radiation at Barrow, FIRE ACE provided in situ aircraft measurements during the 4-month period to improve satellite retrievals of cloud and surface characteristics in the Arctic, while SHEBA was a 1-yr program to observe the surface energy balance and the sea ice mass balance of the Arctic Ocean (Curry et al. 2000; Randall et al. 1998).

To begin the process of evaluating cloud parameterizations and validating satellite retrievals using data collected at Barrow, we have compiled a 5-month record of single-layer and overcast low-level stratus cloud macrophysical, microphysical, and radiative properties, as well as surface radiation budget and cloud radiative forcing using data collected at the ARM NSA site near Barrow, Alaska, from May to September 2000 (referred to collectively as the summer 2000 results). During this period, the liquid-phase and liquid dominant mixed-phase low-level Arctic stratus clouds occurred frequently, which makes it possible to retrieve their microphysical and radiative properties using the new cloud parameterization (see the appendix). The record of cloud properties provides a unique source of information for studying the seasonal variation of Arctic stratus cloud properties and their impact on the surface radiation budget. In order to establish the representativeness of the datasets collected at Barrow during summer 2000, the cloud properties are compared with aircraft in situ measurements in similar conditions (Lawson et al. 2001; Hobbs et al. 2001; Dong et al. 2001), surface observations (Intrieri et al. 2002a,b; Curry et al. 2001), and satellite data (Minnis et al. 2001; Maslanik et al. 2001) during the FIRE ACE and SHEBA field experiments. We also compare the summer 2000 results with the aircraft in situ measurements collected over the Beaufort Sea during the Arctic Stratus Clouds (ASC) experiment in June 1980 (Herman and Curry 1984; Tsay and Jayaweera 1984) and the Beaufort and Arctic Storms Experiment (BASE) in autumn 1994 (Pinto et al. 2001), as well as from Hobbs and Rangno's study in June 1995 (Hobbs and Rangno 1998). Although these comparisons are based on data collected at different locations and different years, this allows us to pose the following two questions:

1) What is the seasonal variation of Arctic stratus cloud macrophysical, microphysical, and radiative properties at Barrow, Alaska, from spring to autumn? How and when does this seasonal variation of cloud properties influence the surface radiation budget?
2) How well do the summer 2000 results, generated at a single point over one summer, represent the western Arctic summer climatology? For example, what are the differences in the cloud properties and associated radiative forcing between Barrow and the SHEBA ship? Does the cooling effect of clouds vary in duration and strength at the two sites?

2. Data

The datasets in this study are collected from direct surface measurements or derived from surface measurements, as well as calculated from a new parameterization developed from an existing cloud property retrieval algorithm (see the appendix). The surface observations at the ARM NSA site in this study are listed in Table 1. The millimeter wavelength cloud radar (MMCR; Moran et al. 1998) is the centerpiece of this instrument array. The MMCR operates at a wavelength of 8 mm in a vertically pointing mode, and provides continuous profiles of radar reflectivity from hydrometeors advecting through the radar field of view allowing us to identify clear and cloudy conditions. The cloud-top height (Z_{top}) is derived from the MMCR reflectivity profile, and the cloud-base height (Z_{base}) is derived from laser ceilometer measurements. Since the laser ceilometer is sensitive to the second moment of the particle distribution instead of the sixth moment like the MMCR, the ceilometer provides a more faithful estimate of cloud base. The temporal and vertical resolutions and maxi-

TABLE 1. Summary of surface instruments at the ARM NSA site.

Instrument	Temporal resolution (s)	Vertical resolution (m)	Range (km)	Observed/derived cloud parameters
Cloud radar	10	45	Up to 20	Cloud heights, profiles of radar reflectivity, Doppler velocity and spectral width
Ceilometer	30	7.6	Up to 7.5	Cloud-base height
Rawinsonde	1 day^{-1}	5	Up to 25	Profiles of pressure, temperature, and relative humidity
Microwave radiometer	300	N/A	N/A	Column-integrated liquid water and water vapor
PSP pyranometer	60	N/A	N/A	Downward/upward broadband SW flux
PIR pyrgeometer	60	N/A	N/A	Downward/upward broadband LW flux

mum detected heights of the MMCR and ceilometer are also listed in Table 1. The total and low-level cloud fractions are averaged over 10-day intervals from the combined measurements of the MMCR and ceilometer as the fraction of time that the upward-looking narrow field-of-view radar and ceilometer detected clouds. The total cloud fraction is the fraction of time cloud detected anywhere in the vertical column, and the low-level cloud fraction is the fraction of time low cloud ($Z_{\text{top}} < 3$ km) detected during a 10-day period. The cloud fraction discussed here should not be confused with an instantaneous hemispheric cloud fraction used in radiative calculations and reported in surface observations. Averaged over a long time period, the two definitions tend to converge, however. Values of cloud base and top temperatures (T_{base} and T_{top}) are found from ARM NSA rawinsonde soundings (launched once per day at around local noon) using Z_{base} and Z_{top} derived from the ceilometer and radar data.

The cloud liquid water path (LWP) is derived from microwave radiometer brightness temperatures measured at 23.8 and 31.4 GHz using a statistical retrieval method (Liljegren et al. 2001). The root-mean-square (rms) accuracies of the retrievals are about 20 g m^{-2} and 10% for cloud LWP below and above 200 g m^{-2}, respectively (Dong et al. 2000, hereafter D00; Liljegren et al. 2001). This retrieval method (Liljegren et al. 2001) may overestimate the LWP of supercooled clouds (Westwater et al. 2001) due to poorly known absorption coefficients and an incorrect treatment of the cloud liquid dielectric model. However, the overestimation of LWP ($\sim$10–20 g m^{-2}) is within the expected accuracy of the retrievals (J. Liljegren 2001, personal communication), and its influence on the retrieved effective radius is also within the uncertainty of the retrieved effective radius (Dong et al. 1997, 1998; hereafter D97, D98). Therefore, the low limit of LWP is set to 20 g m^{-2} in this study.

The up- and down-looking standard Eppley precision spectral pyranometers (PSPs) and precision infrared radiometers (PIRs) (pyrgeometer) provide measurements of downward and upward broadband shortwave (0.3–3 μm) and longwave (4–50 μm) fluxes at the surface, respectively. The absolute accuracies of the PSP and PIR measurements are approximately 10 W m^{-2} (Long and Ackerman 2000). The surface albedo (R_{sfc}) is derived from the ratio of upward to downward shortwave flux measurements. The effective solar transmission (γ) is the ratio of the measured cloudy downward shortwave flux at the surface to the inferred clear-sky downward shortwave flux that would be recorded by the broadband pyranometer if there were no clouds. Long and Ackerman (2000) first fit the downward shortwave flux measurements on the clear-sky days that are closest in time to the cloudy days, and then interpolate the empirical curve-fitting values to cloudy days to estimate clear-sky downward shortwave fluxes that would be observed under the assumption of constant aerosol optical depth during this time period. The aerosol optical depth can vary by a factor of 4 over a short period of time during Arctic haze events (which are common in spring) when the aerosol optical depth can be as high as 0.5 (e.g., Stone 1997). These variations may have a significant impact on the inferred clear-sky shortwave flux and thus affect the retrievals of cloud properties. Strictly speaking, the inferred clear-sky downward shortwave fluxes on the cloudy days are not measurements; nonetheless, they are derived from the measurements and should be more appropriate than model calculations in estimation of γ because the estimated clear-sky values automatically incorporate any biases between measured and modeled surface downward shortwave fluxes (Kato et al. 1997). The γ increases with increased R_{sfc} because the PSP-measured cloudy downward solar flux at the surface includes the multiple reflections of solar radiation between the cloud layer and the highly reflective surface (see Fig. A1 of the appendix).

The cloud-droplet effective radius (r_e), number concentration (N), broadband shortwave optical depth (τ), and bulk albedos at the top of cloud and atmosphere (R_{cldy}, R_{TOA}) with the underlying reflecting surface are calculated by the new cloud parameterization. The new cloud parameterization is the same as that described by D98 except the impact of surface albedo is included. More details about the retrieval method and old/new cloud parameterizations are discussed in the appendix. The uncertainties in τ, R_{cldy}, and R_{TOA} are generally less than 5%, while in r_e and N they are about 10 and 30%, respectively (D97; D98).

3. Results

We have established five criteria for choosing the clouds under which cloud properties can be estimated

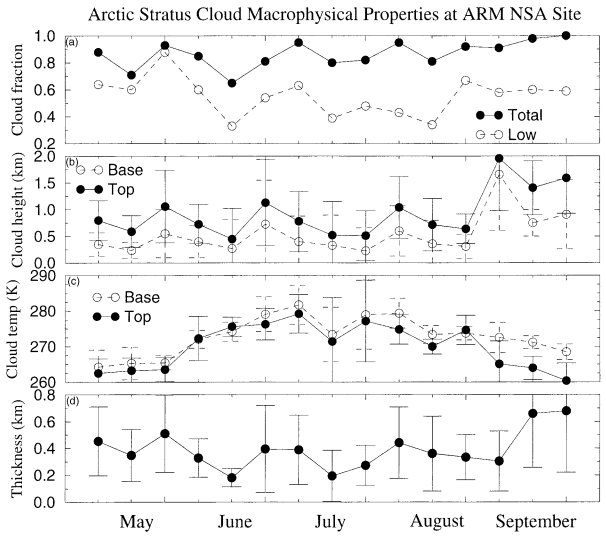

FIG. 1. The 10-day means (std devs) are simply the averages of all samples (5-min resolution) for (a) total and low cloud fractions, and the selected samples using the five criteria for (b) cloud-base and -top heights, (c) temperatures, and (d) cloud thickness in km within a 10-day period. The cloud-base and -top heights are derived from the radar and ceilometer measurements, respectively, and cloud-base and -top temperatures from the ARM NSA rawinsonde soundings (~local noon) using the ceilometer and radar-derived cloud-base and -top heights.

using the new cloud parameterization. These criteria are (i) only single-layer and overcast low-level stratus clouds are present as determined from cloud radar observations, (ii) the cosine of solar zenith angle (μ_0) is larger than 0.2, (iii) the range of γ is between 0.1 and 0.8, (iv) LWP is between 20 and 600 g m^{-2}, and (v) Z_{top} is less than 3 km. The physical reasons for using these five criteria were discussed in D00. We identified approximately 300 h of the stratus clouds (more than 3600 samples at 5-min resolution) that satisfied these five criteria during the study period, which include the retrieved cloud parameterization and the measured or derived cloud quantities from surface observations. The retrievals consist of cloud-droplet effective radius (r_e) and number concentration (N), broadband shortwave optical depth (τ), and bulk albedos at the top of cloud and atmosphere (R_{cldy}, R_{TOA}) with the underlying reflecting surface. The measured or derived cloud quantities include cloud-base/top heights ($Z_{\text{base}}/Z_{\text{top}}$) and temperatures ($T_{\text{base}}/T_{\text{top}}$), cloud-layer geometric thickness (ΔZ), cloud LWP and liquid water content (LWC), effective solar transmission (γ), surface albedo (R_{sfc}) with a cloud above, and cloudy net shortwave (SW) and longwave (LW) fluxes. Other cloud elements, including total and low-level cloud fractions (C_{tot}, C_{low}) and clear-sky net SW and LW fluxes, are compiled irrespective of the five conditions listed above.

As shown in Fig. 1, clouds were dominant at the NSA site during the study period, thus there were only limited LW and SW flux measurements for clear-sky conditions during any 10-day period. The averaged clear-sky LW flux may provide a representative value of the 10-day clear-sky LW flux because LW flux does not change too much for the daytime. However, SW flux is strongly dependent on solar zenith angle so that the averaged clear-sky SW flux from the limited samples during a 10-day period cannot represent real clear-sky information. Therefore, we use the empirical curve-fitting technique to infer clear-sky downward SW flux, and then use it with all-sky (clear and cloudy) measured R_{sfc} to infer clear-sky upward SW flux. We note that all-sky R_{sfc} is slightly different from clear-sky R_{sfc}, but this appears to be the most reasonable approach to inferring the clear-sky SW fluxes for conditions that are predominantly cloudy. The clear-sky net LW and SW fluxes are deduced from the difference between downward and upward fluxes for $\mu_0 > 0.2$ during the 10-day period to be consistent with the cloudy net fluxes. The clear-sky values are then used to derive LW and SW cloud radiative forcings.

a. Macrophysical properties

The 10-day means and standard deviations of cloud macrophysical properties from May to September 2000 at the ARM NSA site are shown in Fig. 1, and the corresponding frequency distributions during the 5-month period are shown in Fig. 2. These means (standard deviations) are simply the averages of all samples (5-min temporal resolution) within a 10-day period. The averaged C_{tot} during the 5-month study period is 0.87 with a maximum of 0.96 in September and a minimum of 0.77 in June, and the averaged C_{low} is 0.55 with a maximum of 0.69 in May and a minimum of 0.47 in June. From high values of total and low-level cloud fractions, we can draw a conclusion that the ARM NSA site is an ideal location to study clouds, especially low-level stratus clouds. The 10-day averaged Z_{base} and Z_{top} altitudes are, in general, around 0.4 and 0.8 km, leading to a ΔZ of 0.4 km. From the frequency distributions, most Z_{base} values are less than 1 km with a mean value of 0.47 km and a standard deviation of 0.56 km, and most Z_{top} values are less than 1.5 km and have a broad frequency of occurrence histogram. Most T_{base} and T_{top} values are above 0°C from late June to early September, whereas others range from −10° to 0°C with liquid dominant mixed-phase stratus clouds.

b. Microphysical properties

The 10-day means and standard deviations of cloud microphysical properties are shown in Fig. 3, and the corresponding frequency distributions are also shown in Fig. 2. Most 10-day averaged cloud LWPs range from 50 to 150 g m^{-2}, and more than 85% of the cloud LWPs are less than 150 g m^{-2} with a mean and standard deviation of 91 and 67 g m^{-2}, respectively. Cloud LWC is the ratio of cloud LWP to ΔZ. The 10-day means of

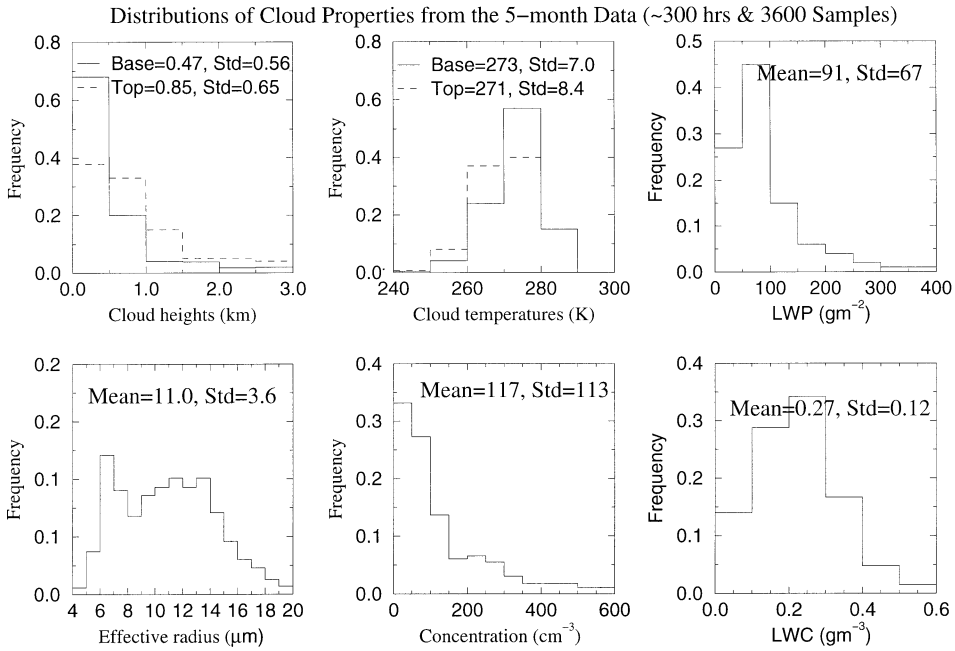

FIG. 2. Frequency distributions of the selected cloud macrophysical and microphysical properties using the five criteria during May–Sep 2000 at the ARM NSA site.

cloud LWC increase from early May (0.2 g m^{-3}) to the summer (0.35 g m^{-3}), then decrease to 0.2 g m^{-3} in late September. Thus, cloud LWC during the summer 2000 at the NSA site increases with increased cloud mean temperature. This positive correlation (0.31) between LWC and cloud mean temperature is not found using data collected at the ARM Southern Great Plains (SGP) site (36.6°N, 97.5°W) (D00). We find no correlation between cloud LWP and cloud temperature in this study nor is this correlation found at the ARM SGP site (Table 2 in D00). These findings are based on 10-day means in this study and monthly means at the ARM SGP site and therefore should be viewed with caution. The only difference between these two quantities (LWP and LWC) is the cloud geometric thickness. This suggests that warmer cloud layers are thinner but contain higher LWC than colder layers at the ARM NSA site, not at the ARM SGP site. The difference in the relationships between cloud thickness and temperature at the NSA and SGP sites may reveal that the formation, maintenance, and dissipation processes of stratus clouds in the midlatitudes and Arctic are different. Preliminary calculations suggest these correlations are lower at higher temporal resolution and additional study is ongoing to explain these findings.

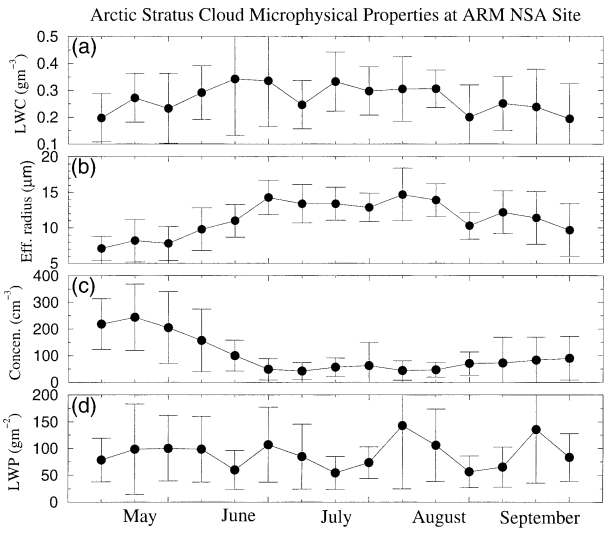

FIG. 3. Ten-day averages and standard deviations of cloud parameters based on the 5-min-averaged samples selected using the five criteria described in the text. (a) Cloud LWC derived from the ratio of LWP to ΔZ, (b) cloud-droplet effective radius, and (c) number concentration calculated from the new cloud parameterization. (d) Cloud LWP retrieved from microwave radiometer measured brightness temperature.

The 10-day means and standard deviations of r_e and N are illustrated in Fig. 3, and their frequency distributions are also shown in Fig. 2. The means of r_e monotonically increase from early May to mid June, then begin to decrease in August. Overall, r_e is larger during the summer than in the spring and autumn. As Fig. 2 demonstrates, most effective radii range from 4 to 16 μm with a bimodal distribution. The small and large modes appear to peak at 6–7 μm and 11–14 μm, respectively. The smaller particle mode mainly consists of clouds that were observed during the spring and autumn, while the larger particle mode is mostly from the clouds observed during the summer. The variation of N

TABLE 2. Monthly averaged values of cloud properties at the ARM NSA site.

	May	Jun	Jul	Aug	Sep
C_{tot}	0.83	0.77	0.86	0.89	0.96
C_{low}	0.69	0.47	0.50	0.48	0.59
Z_{base}, km	0.389	0.431	0.297	0.393	1.059
Z_{top}, km	0.830	0.736	0.591	0.762	1.608
T_{base}, K	265.1	274.1	278.3	274.9	271.3
T_{top}, K	263.2	273.9	276.1	272.9	264.0
LWP, g m^{-2}	94.1	89.6	74.8	94.6	107.4
LWC, g m^{-3}	0.237	0.308	0.291	0.263	0.237
r_e, μm	7.77	11.03	13.39	12.6	11.45
N, cm^{-3}	222.4	121	53.9	56.2	81.4
τ	17.7	12.5	8.6	10.9	13.8
γ	0.688	0.576	0.544	0.448	0.465
R_{cldy}	0.852	0.739	0.553	0.623	0.729
R_{TOA}	0.703	0.611	0.457	0.514	0.602
R_{sfc}	0.860	0.589	0.172	0.157	0.432
SW_{clear}	70.0	263.1	370.3	319.2	161.3
SW_{cloud}	42.4	110.8	203.7	145.3	74.6
LW_{clear}	−51.7	−70.5	−101.8	−102.9	−94.1
LW_{cloud}	−12.1	−19.0	−32.4	−26.7	−26.2
CRF_{SW}	−27.6	−152.3	−166.6	−173.9	−86.7
CRF_{LW}	39.6	51.5	69.4	76.2	67.9
CRF_{NET}	12.0	−100.8	−97.2	−97.7	−18.8

is always complementary to that of r_e with much smaller values during the summer than in the spring and autumn (Fig. 3). More than 70% of the N values are less than 150 cm^{-3} with a mean and standard deviation of 117 and 113 cm^{-3}, respectively. During the summer, the means of r_e and N are around 13 μm and 60 cm^{-3}, which are the same as midlatitude marine stratus cloud microphysical properties (D97). While during the spring and autumn seasons, the means of r_e vary from 7 to 10 μm, and the N values are around 200 cm^{-3}—similar to midlatitude continental stratus clouds (D97; D98; D00; Mace and Sassen 2000; Dong et al. 2002).

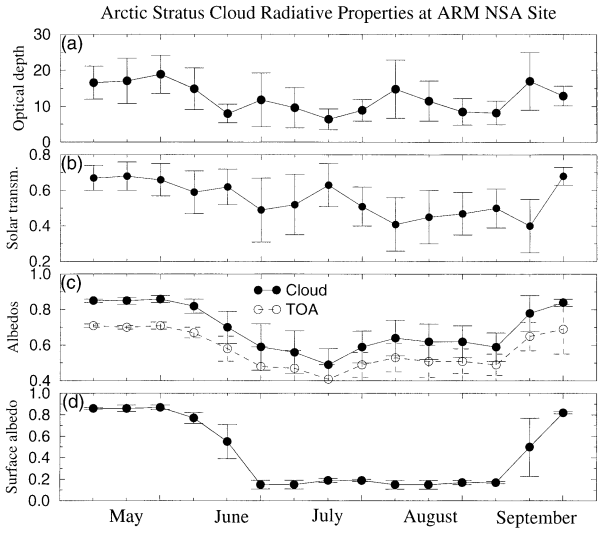

FIG. 4. 10-day averages and standard deviations derived from the 5-min-averaged samples selected using the five criteria. (a) Cloud optical depth, (c) cloud and TOA albedos calculated from the new cloud parameterization, and (b) effective solar transmission, and (d) surface albedo derived from the PSP measurements.

We note that the variations of r_e and N, as discussed above, are similar to that reported in D00 using data collected at the ARM SGP site. This suggests that similar seasonally varying factors may be influencing the cloud microphysical properties at the two sites. These factors include the increased levels of absolute humidity in the warmer temperatures, more vigorous boundary layer dynamics due to solar heating, and/or a decrease in the strength of the inversion near cloud top. Aerosol effects may be another factor for the variation of cloud microphysics at the NSA site as we discussed in section 2. Factors that may lead to the seasonal variation of cloud microphysics are discussed in the next section. We now demonstrate how this seasonal cycle in cloud microphysics influences the seasonal variation of cloud radiative properties.

c. Radiative properties

The calculated broadband cloud optical thickness (τ), and bulk albedos at the top of cloud and atmosphere (R_{cldy}, R_{TOA}), as well as the PSP-derived effective solar transmission (γ) and surface albedo (R_{sfc}) are illustrated in Fig. 4, and their frequency distributions are shown in Fig. 5. The R_{sfc} values in May are more than 0.8, then decrease significantly from the beginning to the end of June, and keep nearly a constant value of 0.16 for the whole summer, and finally increase from early to late September (0.8). The large standard deviation of R_{sfc} in mid June suggests that snow melted quickly in that time period, while the first snow of the coming winter occurred in the middle of September. With a snow-covered

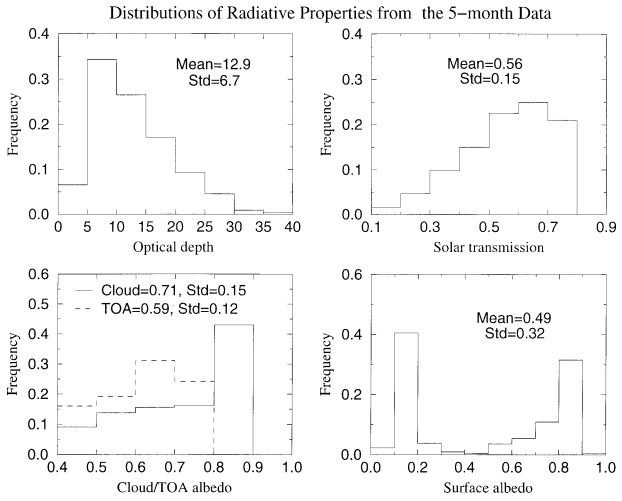

FIG. 5. Frequency distributions of the selected cloud radiative properties (~300 h and 3600 samples in 5-min resolution) using the five criteria between May and Sep 2000 at the ARM NSA site.

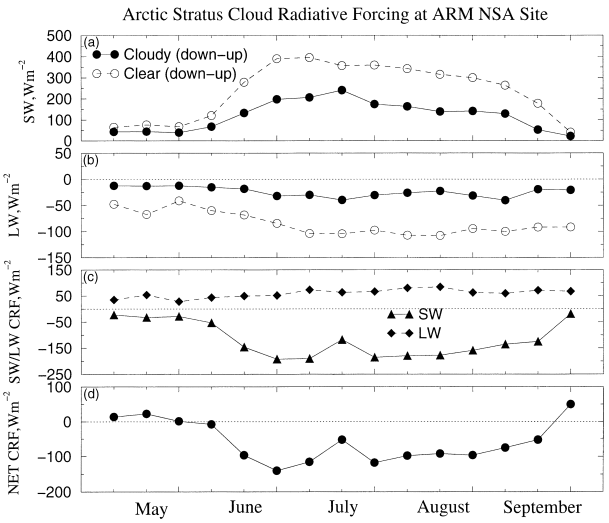

FIG. 6. The 10-day means of (a) SW and (b) LW fluxes; the clear-sky net LW and SW fluxes are calculated from pyrgeometer measurements and inferred SW flux, respectively, for the daytime ($\mu_0 > 0.2$) during the 10-day period. The 10-day means of cloudy net SW and LW fluxes are the averages of the selected samples using the five criteria. (c) The 10-day SW (LW) CRF is the difference between cloudy and clear-sky net SW (LW) 10-day means, and (d) the 10-day net CRF is the summation of SW and LW CRFs (the values of net CRF are negative for cooling and positive for warming of the surface).

surface, the cloudy-sky surface albedo is approximately 5% higher than the clear-sky surface albedo because snow reflects diffuse solar radiation better than direct solar radiation and clouds attenuate near-IR radiation more efficiently than visible radiation.

The variations of the 10-day means of R_{cldy} and R_{TOA} basically follow the trend of R_{sfc}. These results confirm that R_{cldy} and R_{TOA} depend on both τ and R_{sfc}. During summer both R_{cldy} and R_{TOA} are mainly determined by τ, and do not depend on R_{sfc} because R_{sfc} is low and constant. As Fig. A1 (in the appendix) demonstrates, the dependence of R_{cldy} on τ becomes smaller with increased R_{sfc} for nonabsorbing cloud. This argument has been confirmed by the R_{cldy} values in mid- and late September periods where τ is smaller and both R_{cldy} and R_{sfc} are larger in late September than in mid September. The variation in the 10-day means of τ follows the variation of LWP, and most of the τ values are between 5 and 20 with a mean value of 12.9 (Fig. 5). Only 6% of the τ values are less than 5, which are mainly due to the selection criteria (iii) and (iv) listed in the beginning of this section. Here γ is negatively correlated to τ for low R_{sfc}, but this correlation is significantly modified under a snow-covered surface. For instance, the τ (~15) in early June is almost double the value (~8) in mid June, whereas the γ values in these two periods are nearly the same. This is mainly due to the R_{sfc} difference where the former R_{sfc} (0.74) is about 50% higher than the latter R_{sfc} (0.49). The higher R_{sfc} results in more multiple reflections of solar radiation between the cloud layer and the highly reflecting surface, which ultimately results in higher γ.

The importance of r_e and R_{sfc} to R_{cldy} is demonstrated in the appendix (Fig. A2). For fixed LWP, R_{cldy} has a significant dependence on both r_e and R_{sfc}. The seasonal variation of cloud microphysics, small (large) $r_e(N)$ during the spring and large (small) $r_e(N)$ during the summer in this study, strongly supports the seasonal variation of R_{cldy} (high in spring and low in summer). It appears that R_{cldy} is significantly affected by the cloud properties during the summer when R_{sfc} is relatively small, but not during the spring because R_{cldy} is insensitive to cloud optical depth when R_{sfc} is large (Figs. A1 and A2).

d. Surface cloud radiative forcing

The change in the surface radiation balance due to clouds is termed cloud radiative forcing (CRF). The CRF is classified into shortwave (CRF_{SW}) and longwave (CRF_{LW}) and defined as (Ramanathan et al. 1989; Curry et al. 1996)

$$\text{CRF}_{\text{SW}} = Q_1 - Q_0, \qquad \text{CRF}_{\text{LW}} = F_1 - F_0. \quad (1)$$

The CRF is the difference between the flux when skies are overcast (Q_1 and F_1, cloud fraction = 1) and when they are clear (Q_0 and F_0, cloud fraction = 0), and Q and F are the net (downward minus upward) SW and LW fluxes. The net CRF, CRF_{NET}, is the sum of CRF_{SW} and CRF_{LW} at the surface. The values of CRF are positive for warming of the surface and negative for cooling of the surface.

The cloudy and clear-sky net SW and LW fluxes, and the SW/LW/net CRFs are shown in Fig. 6, where the filled circles represent the averaged cloudy net SW and LW fluxes in a 10-day period, and open circles represent the averaged clear-sky net SW and LW fluxes in that period in the two upper panels of Fig. 6. As Fig. 6

demonstrates, both cloudy and clear-sky net SW fluxes are relatively small ($\sim$50 W m^{-2}), and the clear-sky net SW flux is only slightly larger than the cloudy net SW flux when R_{sfc} is large. However, during the summer when R_{sfc} is small, both cloudy ($\sim$100–200 W m^{-2}) and clear-sky ($\sim$300–400 W m^{-2}) net SW fluxes are large with a peak during late June–early July. During this time period, the clear-sky net SW flux is much larger than the cloudy net SW flux showing that the SW cooling effect of Arctic stratus is obvious and dominant at Barrow. The cloudy net LW flux is nearly constant and around -20 W m^{-2} while the clear-sky net LW flux decreases approximately from -50 W m^{-2} in May to -100 W m^{-2} in July due to the significant increase in surface temperature that results in increasing upward LW flux. The surface temperature is nearly equal to the cloud-base temperature because the surface is in the thermal equilibrium with the clouds. This is particularly true for the overcast, optically thick cloud conditions used in this study. The surface does warm when clouds are not present because of solar heating.

Compared to the SW CRFs, the LW CRFs maintain relatively small positive values and vary slightly during the 5-month period. The LW CRFs range from around 40 W m^{-2} in May to 70 W m^{-2} during July–August, while the SW CRFs vary from -30 W m^{-2} in May to -170 W m^{-2} during July–August, and then return to -30 W m^{-2} in September. The net CRFs drop from a small positive value ($\sim$10 W m^{-2}) in May to a large negative value (-100 W m^{-2}) in the summer, and then return to near the springtime values in September. The variation of net CRFs is mainly determined by the SW CRFs and the trend of net CRF variation is nearly the same as that of R_{sfc} except during the middle of July. During the summer, R_{sfc} is low and the net CRF values are large but negative—a strong cooling effect that is similar to low and middle latitude stratus clouds (Ramanathan et al. 1989; Harrison et al. 1990; Hartmann et al. 1992). During the spring and autumn seasons, the SW CRFs are small and the LW CRFs are the dominant factor in the net CRFs. The positive net CRFs during the spring and autumn seasons suggest that Arctic stratus clouds have a warming effect on the surface relative to a cloudless atmosphere. The warming effect of clouds in spring will tend to enhance snow melting and in fall it may slow the solidification of the permafrost.

Understanding the impact of cloud properties on the surface energy balance is not always straightforward, however. For example, all net CRFs (Fig. 6) during the summer are around -100 W m^{-2} except the middle of July. During the summer, all τ values are more than or around 10 except during the period of mid July ($\sim$6) when optically thinner layers allow some direct solar flux to penetrate to the surface. Therefore, the SW CRF has a small negative value that results in a small negative net CRF during that period. The reason leading to the bump of net CRF in mid July is mainly due to our selection criterion (iii) where the range of γ is between 0.1 and 0.8 in this study. In all previous studies, the maximum of γ was set to 0.7 ensuring that only diffuse solar radiation was recorded by the ground-based solar radiometers. The maximum of 0.8 in this study is reasonable to account for the multiple reflections of solar radiation between the cloud layer and the highly reflective snow/ice surface, in which the diffuse solar transmission is still dominant. However, for lower R_{sfc} during summer, the maximum of 0.8 results in the inclusion of some situations where direct solar flux contributes to the ground-based PSP observations. The apparent anomaly in the middle of July includes a significant number of such cases. If we set the maximum of γ to 0.7, the new net CRF will be -96 W m^{-2} for that period, which is much more negative than the original value (-52 W m^{-2}) and also much closer to the net CRFs of nearby time periods. This new set ($\gamma_{max} = 0.7$) significantly affects the net CRF calculation in the period of mid July but not for other time periods because the percentage of $\gamma > 0.7$ is more than 35% for that period, while it is less than 5% for other 10-day periods during the summer. However, many cloud samples during the spring and autumn periods would be missed if the maximum of γ were set to 0.7. Therefore, we still use $\gamma_{max} = 0.8$ in this study.

The bump of net CRF in mid July also suggests that there are other factors affecting the net CRF except R_{sfc}, and this motivates us to calculate the correlation coefficients between net CRF and cloud parameters. The correlation coefficients between net CRF and R_{sfc}, γ, and τ from the averages of 15 10-day periods in this study are 0.79, 0.53, and -0.24, respectively. It is straightforward to understand the positive correlation between net CRF and R_{sfc} because the net CRF values are small positive for high R_{sfc} and large negative for low R_{sfc}. The positive (negative) correlation between net CRF and $\gamma(\tau)$ also appears reasonable because a low (large) solar transmission (optical depth) will result in a small cloudy net SW flux and a large negative net SW CRF, and therefore a large negative net CRF. A more complete understanding of the quantitative correlations between the SW/LW/net CRFs and the cloud parameters should be determined from higher temporal resolution data, such as hourly or daily, rather than 10-day averages and by examining the meteorological situations that contribute to the formation and maintenance of cloud fields in this region.

e. Summary

The single-layer and overcast low-level Arctic stratus macrophysical, microphysical, and radiative properties, as well as surface radiation budget and cloud radiative forcing at the ARM NSA site are summarized as a function of month in Table 2. Both C_{low} and C_{tot} have a minimum in June and their maxima are in May and September, respectively. Most values of Z_{base} are around 0.4 km and Z_{top} are 0.8 km except in September where

both Z_{base} and Z_{top} values are more than 1 km. Both T_{base} and T_{top} increase more than 10 K from the spring to the summer where the Arctic stratus has changed from liquid-dominant mixed phase to liquid phase only. The r_e and N values in the spring are similar to midlatitude continental stratus cloud microphysical properties (D00), and in the summer they are similar to midlatitude marine stratus clouds (D97). Here R_{cldy} and γ depend on both τ and R_{sfc} when R_{sfc} is high. If we define the significant time periods at the ARM NSA site based on this study, from May to mid June is the transition period of spring melting, from late June to early September is summer, while the transition period to autumn freezing started in mid September during the year 2000. During the summer, Arctic stratus clouds have a strong cooling effect on the surface while during the spring and autumn periods, they have a slight warming effect at the ARM NSA site.

4. Discussion and comparisons with other datasets

To determine how well the data collected at Barrow and analyzed in this study represent cloud properties in the western Arctic region, it is necessary to compare with other field observations. Therefore, we compare the summer 2000 results with aircraft in situ measurements (Lawson et al. 2001; Hobbs et al. 2001; Dong et al. 2001), surface observations (Intrieri et al. 2002a,b, Curry et al. 2001), and satellite retrievals (Minnis et al. 2001; Maslanik et al. 2001) during the FIRE ACE and SHEBA experiments. We also compare with aircraft in situ measurements collected over the Beaufort Sea during the ASC experiment in June 1980 (Herman and Curry 1984; Tsay and Jayaweera 1984) and the BASE experiment in autumn 1994 (Pinto et al. 2001), as well as from Hobbs and Rangno's study in June 1995 (Hobbs and Rangno 1998). Although these comparisons are based on data collected at different locations and years, it is instructive to consider the similarities and differences between the ARM NSA results and data collected in other field campaigns.

a. Cloud formation, maintenance, and dissipation processes

Paluch and Lenschow (1991), based on aircraft in situ measurements, developed a conceptual model of the life cycle of a marine stratus layer in the midlatitudes. It starts initially as a thin, homogenous layer, then grows and becomes patchy with time and produces precipitation. This stage is followed by the formation of small cumuli below and eventually disintegrates, leaving a field of cumuli behind. The summer stratus clouds at the ARM SGP site (36.6°N, 97.5°W), based on the 25-month datasets in the D00 study, normally form in the morning and dissipate in the afternoon due to strong solar heating at the surface, and the lifting of entire cloud layer from morning to afternoon. The life cycle of a stratus cloud event at the ARM SGP site is similar to the conceptual model generated by Paluch and Lenschow (1991) except that the end result is normally dissipation without precipitation.

By contrast, a summer Arctic stratus event at the ARM NSA site tends to last at least a few days, and even more than 10 days as we found in this study. It is apparent that the formation, maintenance, and dissipation processes of Arctic stratus clouds are significantly different from what typically occurs at the SGP site or was hypothesized in the conceptual models. Arctic stratus clouds are formed very near the sea-ice surface if warm moist air advects over the cold Arctic Ocean, or by a convective-type process if cold polar air flows over a warmer sea-ice surface (Tsay and Jayaweera 1984). As Herman and Goody (1976) pointed out, once Arctic stratus clouds form, they persist. This is the significant difference between the Arctic and midlatitude stratus clouds. In the Arctic the dissipative mechanisms found in the midlatitudes such as precipitation, convective heating from the surface, absorption of solar radiation, and destruction by synoptic activity are either nonexistent or relatively weak. The persistence of the cloud field occurs in a steady-state situation where dissipative processes are balanced by advection of air masses into a region where the synoptic regimes are suitable for cloud formation and maintenance. Certainly further study is required to more fully understand these feedbacks and eventually parameterize these physical processes in large-scale models.

b. Cloud fraction

Cloud fraction for the surface observer is the percentage of the sky dome covered by clouds, while for the satellite imager, it is the ratio of the number of pixels classified as cloudy to the total number of pixels within some defined earth surface area. Cloud fraction derived from lidar and/or radar measurements is simply the percentage of returns that are cloudy within a specified sampling time period. If all three measurements are taken at the same time with some time allowance for building a set of returns for lidar/radar estimate, it is unlikely that they will agree completely for a given observation unless there are extensive overcast or clear skies. Each viewing perspective provides an estimate for a unique area that may contain a different fractional cloudiness. However, if it is assumed that the cloud cover, when averaged over a sufficient time interval, is essentially invariant over a relatively large area (e.g., 100-km wide) then the mean values from all three sensors should agree if each provides an accurate representation of the mean cloud fraction.

The monthly averaged total cloud fractions derived in this study and during the FIRE ACE and SHEBA experiments are listed in Table 3. The monthly averaged cloud fractions from the surface observers are based on 6-hourly visual observations (Minnis et al. 2001; Mas-

TABLE 3. Comparison of monthly averaged total cloud fractions at the ARM NSA site and SHEBA ship.

Location	Observation	Source	May	Jun	Jul	Aug	Sep
ARM	Sfc radar/lidar	This study	0.83	0.77	0.86	0.89	0.96
ARM	Sfc observation	Chakrapani et al. (2001)	0.91	0.82	0.69		
ARM	AVHRR	Chakrapani et al. (2001)	0.89	0.83	0.65		
SHEBA	Sfc radar/lidar	Intrieri et al. (2002b)	0.88	0.87	0.94	0.92	0.97
SHEBA	Sfc observation	Minnis et al. (2001)	0.76	0.76	0.87		
SHEBA	AVHRR	Minnis et al. (2001)	0.71	0.75	0.84		
SHEBA	AVHRR	Maslanik et al. (2001)	0.93	0.88	0.78		

lanik et al. 2001). The monthly averaged cloud amounts derived by Minnis et al. (2001) over the Beaufort Sea and by Chakarapani et al. (2001) over the ARM NSA site during FIRE ACE from the Advanced Very High Resolution Radiometer (AVHRR) High-Resolution Picture Transmission 1-km satellite images vary, on average, by about 6%/100 km. Thus, comparisons of monthly averaged cloud fraction should be sufficient to determine the relative accuracies of the various cloud amounts to within $\pm 3\%$. The cloud fractions derived from *NOAA-12* and *NOAA-14* AVHRR data (Minnis et al. 2001) are averaged over the Arctic Ocean for a 25-km radius centered on the SHEBA ship. These two satellites provide good diurnal sampling except between 1800–2400 local time (LT). The cloud fractions derived by Maslanik et al. (2001) are based on the newly available 5-km resolution AVHRR-based Polar Pathfinder products at 1400 LT for the 105 km $\times$ 105 km region centered on the SHEBA ship.

It is noted that the monthly averaged cloud fractions derived from the SHEBA radar/lidar pair are generally higher than those derived from the ARM NSA radar/ceilometer pair. This difference may be partially real owing to differences in location and year (surface types, air masses, annual variability, etc.) and partially an artifact of different sampling. This is not surprising because the clouds are identified by both radar and ceilometer in this study, while by either radar or lidar in the Intrieri et al. (2002b) study. Some of the optically thin clouds may be too thin to be detected by radar (and satellite) but have been detected by lidar due to the different sensitivities of radar and lidar to clouds. Radar is sensitive to the sixth moment of particle distribution while lidar is sensitive to the second moment (D97; Intrieri et al. 2002b). The difference of cloud fraction between Minnis and Maslanik's studies is probably due to (i) the retrieval technique, (ii) temporal sampling (0000–1800 LT vs 1400 LT), and (iii) spatial sampling (a 25-km radius vs 105 km $\times$ 105 km).

Overall, the comparison of cloud fractions between this study and FIRE ACE and SHEBA experiments agree reasonably well and show that the monthly averaged total cloud fractions observed during the two field programs are similar to one another. We do not expect to have a perfect quantitative match from this comparison; rather, we expect to have an agreement in variability for both clear and cloudy periods from a statistical point of view.

c. The climatology of aerosol characteristics and their trajectories

In general, the aerosol concentration in the NSA region from January to April is at a maximum with a source that is largely traceable to man-made pollutants. During May and June a second peak in aerosol concentration is found due to increased phytoplankton activity, while in late summer and early autumn, the concentration tends to be at a minimum due to efficient scavenging by precipitation during the summer months (Pinto et al. 2001; Barrie 1986; Bigg 1980). Harris and Kahl (1994) used a new isentropic air trajectory model to produce 10-day back trajectories that arrived at near-surface altitudes above Barrow during 1985–92. They found that the atmospheric flow patterns for the period 1985–92 depicted by cluster-mean back trajectories arriving at Barrow were mostly southerly/southwesterly and northeasterly during summer and westerly during winter. The former brought warm moist air to form summer Arctic stratus clouds, while the latter brought polluted air masses to the NSA region from north central Russia contributing to Arctic winter pollution and the Arctic haze season. They also found that no pollution was transported from either the contiguous United States or Europe during the 8-yr period.

The climatology of aerosol characteristics in this region and their typical trajectories support our findings—small (large) cloud-droplet effective radius and high (low) concentration occur during the spring (summer) when the aerosol concentration is high (low). Although the studies cited here are not directly related to the same study period, we know of no reason to suspect that their results would not hold generally. Certainly more study is needed to investigate the day-to-day and month-to-month variations of aerosol concentrations at the ARM NSA site and the effect of seasonable variation in aerosol on the microphysical properties of Arctic stratus, and thereby the indirect effect of aerosol on the surface energy balance in this region.

d. Cloud microphysics

In this section, we compare the summer 2000 results with aircraft in situ measurements from the National

TABLE 4. Summary of aircraft in situ measurements collected over the western Arctic region during other field experiments.

Observation	Date (MM-DD-YY)	Time (UTC = LT + 10)	Latitude (°N)	Longitude (°W)	r_e (μm)	N (cm^{-3})	LWC (g m^{-3})
NCAR C-130[a]	5-04-98	23:15–24:15	76.0	165.4	7.9	206	0.32
NCAR C-130[a]	5-15-98	21:50–24:00	76.3	165.3	8.7	59	0.16
NCAR C-130[b]	5-18-98	22:08–22:11	76.0	165.2	N/A	50–150	0.1–0.2
NCAR C-130[a]	5-27-98	22:35–24:20	76.6	168.0	9.1	43	0.09
UW Convair-580	5-29-98	22:11–22:42	76.7	168.1	7.3–15.3	7–50	0.01–0.09
UW Convair-580	6-03-98	21:28–21:29	76.8	167.6	5.5–7.7	65–70	0.03–0.06
UW C-131A	6-06-95	N/A	70.5	145.0	5.3–8.4	20–225	0.19–0.30
UW C-131A	6-14-95	N/A	73.0	147.0	7.4–11.7	63–102	0.16–0.49
NCAR Electra	6-20-80	N/A	72.0–73.8	157.3–159.3	6.5–7.9	178–244	0.15–0.20
NCAR Electra	6-28-80	N/A	77.1–78.0	154.3–155.1	6.2–7.1	220–365	0.15–0.35
NCAR C-130[b]	7-21-98	22:53–23:24	78.3	165.7	N/A	30–60	0.05–0.20
NCAR C-130[b]	7-29-98	22:36–23:05	78.5	163.2	N/A	0–80	0–0.30
NCAR C-130[c]	9-21-94	20:46	73.0–73.1	134.9	8.5	59	N/A
NCAR C-130[c]	10-12-94	21:30–23:56	70.3–72.1	134.8–137.0	9.0–10.5	62–96	N/A

[a]Data from Dong et al. (2001).
[b]Data from Lawson et al. (2001).
[c]Data from Pinto et al. (2001).

Center for Atmospheric Research (NCAR) C-130 (Dong et al. 2001; Lawson et al. 2001) and the University of Washington (UW) Convair-580 (Hobbs et al. 2001) over the SHEBA ship during the FIRE Arctic Clouds Experiment. We also compare with the in situ measurements collected over the Beaufort Sea by the UW Convair C-131A research aircraft in June 1995 (Hobbs and Rangno 1998) and by the NCAR Electra aircraft during the ASC experiment in June 1980 (Herman and Curry 1984). Finally, the cloud microphysics observed by the NCAR C-130 aircraft during the BASE experiment from late September to early October 1994 (Pinto et al. 2001) is also listed in Table 4.

The aircraft results in Dong et al. (2001) were averaged from 1 or 2 h of Forward Scattering Spectrometer Probe (FSSP-100) measurements when the aircraft was within a radius of 10 km of the SHEBA ship. In Lawson's study, LWC was measured by a King hot-wire LWC device and N by an FSSP-100. In Hobbs et al. (2001) and Hobbs and Rangno (1998), the r_e and N values were measured by the same probe, FSSP-100, while the LWC values were observed by the Gerber Scientific Particle Volume Monitor-100 (PVM-100) and the King probe, respectively. The cloud microphysical properties in Herman and Curry (1984) and Pinto et al. (2001) were measured by the Knollenberg FSSP and FSSP-100, respectively.

Comparing Table 4 with Table 2, we find that in all comparisons, one or two parameters of the surface-derived cloud microphysics, such as r_e, N, and LWC, agree with the in situ data but not all at the same time. While it is possible that the discrepancies may be due to instrumental or algorithmic uncertainties, they can also arise from the effects of ice crystals in liquid-dominant clouds, cloud vertical structure that is not totally sampled by the aircraft measurements, and different locations and years. Although these comparisons using the surface and aircraft data are limited, it appears that the surface-retrieved cloud microphysical properties are in reasonable agreement with the aircraft in situ measurements. While it is not possible to validate the surface-retrieved cloud microphysics using the aircraft observations shown in Table 4, the surface retrieval algorithm has been partially validated elsewhere (Dong et al. 1998, 2001). The question we attempt to address with the comparison between Tables 4 and 2 is whether the summer 2000 results fit within the general context of other data collected in the Arctic region.

e. Radiative properties

Using a simple radiation model, Leontyeva and Stamnes (1994) estimated cloud optical depths from ground-based measurements of incoming solar irradiance at Barrow during April–October 1988. The estimations of cloud optical depth were performed for all overcast cloudy conditions based on hourly mean values of incoming and reflected solar irradiances at the surface measured by the pyranometers with the assumptions of plane-parallel and homogeneous cloud layers and fixed r_e ($=7$ μm). The monthly averaged τ values during May–August 1988 were 11, 12, 10, and 20, respectively. The averaged values during June and July are nearly the same as those in this study (Table 2), while the mean value in May is smaller. In August, τ derived by Leontyeva and Stamnes is much higher than the values of other months in their study and the same month in this study.

The monthly averaged surface albedos during May–September 1988, derived from the reflected and incident solar irradiances in Leontyeva and Stamnes's study, are almost the same as those in this study (Table 2). Curry et al. (2001) also presented the $R_{\rm sfc}$ values derived from the surface-based PSP measurements during the FIRE ACE and SHEBA field experiments and showed that surface albedos in May and late September are the same

TABLE 5. Monthly averaged CRFs (W m^{-2}) for all-cloud conditions at the ARM NSA site.

Month	SW_{cloud}	LW_{cloud}	CRF_{SW}	CRF_{LW}	CRF_{NET}
May	55.1	−23.0	−15.0	28.7	13.7
Jun	190.8	−27.8	−72.3	42.7	−29.6
Jul	182.2	−33.0	−188.1	68.8	−119.3
Aug	143.7	−30.4	−175.5	72.5	−103.0
Sep	95.8	−34.6	−65.5	60.0	−6.5

as those in this study and during the summer (July and early August) they are around 0.5. During summer, the difference of R_{sfc} in these two sites is mainly due to the difference in surrounding surface types where the NSA site was covered by low-albedo tundra surrounded by open water (Leontyeva and Stamnes 1994), while the SHEBA ship was covered by a mosaic of low-albedo melt ponds interspersed with much higher albedo regions of ice (Curry et al. 2001).

f. Cloud radiative forcing

Intrieri et al. (2002a) studied an annual cycle of Arctic surface cloud radiative forcing from data obtained during the SHEBA experiment with the same instruments as in this study. The CRF reported in the Intrieri et al. study used the measured fluxes under all-sky conditions, that is, including clear sky, clouds at all levels and fractional amounts. The CRF used in this study is analogous to the maximum CRF defined in the Intrieri et al. study (cloud fraction = 1 for overcast low-level stratus clouds, and cloud fraction = 0 for clear sky). The clear-sky LW and SW fluxes in the Intrieri et al. study were calculated using the Santa Barbara discrete ordinate radiative transfer atmospheric radiative transfer computer code with the inputs of rawinsonde soundings. Since the clear-sky and cloudy fluxes are different between the SHEBA experiment and this study, the comparison of CRF for these two sites should be viewed with caution. The LW CRFs between the ARM NSA site and SHEBA ship are nearly the same, but the values of negative SW CRF at the ARM NSA are much larger than at the SHEBA ship. At the ARM NSA site, the summer cooling period is much longer (2–3 months vs 1–2 weeks), and the summer cooling magnitude is much larger (−100 W m^{-2} vs −5 W m^{-2}) than at the SHEBA ship.

To study the difference of CRFs between all clouds and low-level stratus clouds, we calculated five months of all-cloud CRFs at the ARM NSA site and listed them in Table 5. Comparing to the low-cloud downward LW flux (DLWF), the single-layer cirrus DLWF is lower while the cumulus DLWF is nearly the same. Therefore, the all-cloud net LW fluxes are slightly more negative than those of the low clouds during the 5-month period, which results in smaller LW CRFs for all clouds when the same clear-sky LW flux is used. When cirrus clouds occur over low clouds, the DLWF does not change too much, but the downward SW flux (DSWF) is decreased but not much since most low clouds are already optically thick in this study. Comparing to the low-cloud DSWF, the single-layer cirrus DSWF increases considerably, especially for broken cirrus clouds, while the cumulus DSWF decreases significantly. Therefore the all-cloud SW CRFs are nearly the same as the low-cloud values when the effects of cirrus and cumulus are balanced, and sometimes they do not agree when one of these two clouds dominates.

To further study the impact of surface albedo on the surface radiation budget, we calculate the CRFs of low-level stratus clouds in August at the ARM NSA site with fixed R_{sfc} (=0.5) for both clear and cloudy periods, and compare these results with the SHEBA August CRFs (Intrieri et al. 2002a) as shown in Table 6. Comparing to the original August CRFs at the NSA site, the newly calculated LW CRFs (with fixed R_{sfc} = 0.5) are the same but the SW CRFs are significantly decreased, which results in a small negative net CRF. Comparing to the SHEBA results, the newly calculated LW and SW fluxes and CRFs are much larger (in absolute sense) than those at the SHEBA ship owing to lower solar zenith angle and warmer atmosphere at the NSA site.

g. Summary

The formation, maintenance, and dissipation processes of Arctic stratus clouds are significantly different from midlatitude stratus clouds. In the Arctic the dissipative processes that destroy stratus clouds in the midlatitudes, such as precipitation, convective heating from the surface, and absorption of solar radiation, are often either nonexistent and/or are relatively weak. The comparison of cloud fractions between this study and the FIRE ACE and SHEBA experiments agree reasonably well. For the cloud microphysics, one or two parameters of the surface-derived cloud microphysics (i.e., r_e, N, LWC) in this study agree with the in situ data but not all at the same time. Although these comparisons using the surface and aircraft data are limited, the surface-retrieved cloud microphysical properties in this study agree reasonably well within the range found by aircraft in situ measurements over the western Arctic Ocean during other field experiments. The climatology of Arctic aerosol characteristics and their trajectories shows a

TABLE 6. Monthly averaged CRFs (W m^{-2}) for R_{sfc} = 0.5 (both clear and cloudy sky) in August at the ARM NSA site and SHEBA ship.

Location	SW_{clear}	SW_{cloud}	LW_{clear}	LW_{cloud}	CRF_{SW}	CRF_{LW}	CRF_{NET}
NSA	189.6	87.0	−102.6	−26.7	−102.6	76.2	−26.4
SHEBA	67.2	36.2	−65.3	−11.5	−30.3	55.1	24.8

maximum concentration in winter and a minimum in summer. This is consistent with the seasonal variation of cloud microphysics found in this study. The surface albedos at the SHEBA ship and the ARM NSA site are similar in May and late September because both sites are snow-covered. Comparing the net CRFs at the ARM NSA site with those at the SHEBA ship, the summer cooling period at the ARM NSA site is much longer (2–3 months vs 1–2 weeks), and the summer cooling magnitude is much larger (-100 vs -5 W m^{-2}) than at the SHEBA ship owing to much higher surface albedo and larger solar zenith angle at the SHEBA ship than at the ARM NSA site.

5. Conclusions

A 5-month record of low-level stratus cloud properties (May–September 2000) has been generated to determine the seasonal variation of Arctic stratus cloud macrophysical, microphysical, and radiative properties at the ARM NSA site, and also to examine the impact of stratus cloud properties on the Arctic surface radiation budget. We have also compared the summer 2000 results with datasets collected elsewhere in this region. From the summer 2000 results and comparisons with other datasets, we have found the following:

1) The monthly averaged cloud properties, summarized in Table 2, show that the averaged total and low-level cloud fractions during the study period are 0.87 and 0.55, with minima in June and maxima in May and September, respectively. Almost all low-cloud base heights are around 0.4 km and top heights are 0.8 km, except in September where both Z_{base} and Z_{top} values are above 1 km. Both cloud-base and -top temperatures increase more than 10 K from the spring to the summer. The means of cloud-droplet effective radius and number concentration are close to 8 μm and 220 cm^{-3} during the spring, and 13 μm and 60 cm^{-3} during the summer, respectively. The net cloud radiative forcing cools the surface during the summer and warms the surface during the spring and autumn periods, confirming that Arctic stratus clouds enhance the springtime melting and slow down the autumn freezing of the ice pack compared to having no clouds.
2) The total cloud fractions in this study show good agreement with the satellite and surface results compiled from data collected during the FIRE ACE and SHEBA field experiments in 1998. The cloud microphysics derived from this study, in general, are similar to those collected in past field programs although these comparisons are based on data collected at different locations and years. No attempt has been made to validate the surface-derived cloud properties in this study using aircraft and satellite data. Our goal is to show that the summer 2000 results at the ARM NSA site fit within the general context of other data collected in this region. The surface albedos ($\sim$0.8) at both SHEBA and the NSA site are the same in May and late September. In summer the surface albedo at the ARM NSA site is around 0.2, which is significantly lower than at the SHEBA ship ($\sim$0.5) owing to the different surface types. The summer cooling period at the ARM NSA is much longer and significantly stronger than that at the SHEBA ship. The ARM NSA site seems to represent reasonably well Arctic land areas and adjacent open-ocean regions that transition to low surface albedo and a net negative CRF in summertime, while the SHEBA ship data record represents sea-ice-covered latitudes with larger surface albedo and weaker solar radiation where the net CRF remains weakly positive or neutral during the summer.

The above conclusions are based only on data complied from May to September 2000 at the ARM NSA site, and on comparisons with limited surface, aircraft, and satellite results at different locations and years. No attempt has been made to give an exhaustive climatology of Arctic stratus clouds; rather, our emphasis is to provide fundamental statistical information about Arctic stratus clouds that are useful for improving and/or developing Arctic stratus cloud parameterizations for process models. In order to improve the representation of cloud microphysics and the associated heating and other feedbacks in these models, the actual physical processes that lead to cloud formation and maintenance must be physically understood and parameterized so that the modeled hydrological cycle can faithfully represent what is found in nature. Ultimately, improved parameterizations can only result from a combined effort that builds on the synergy of long-term observations, collocated aircraft data, and satellite data coupled with cloud-resolving models (Krueger 1988), single column models (Randall et al. 1996), and full GCMs.

Acknowledgments. Data were obtained from the Atmospheric Radiation Measurement Program sponsored by the U.S. Department of Energy Office of Energy Research, Office of Health and Environmental Research, Environmental Sciences Division. Special thanks to Ms. J. Intrieri for providing SHEBA CRFs, to Ms. S. Benson for processing the data, and to Drs. Minnis and Coakley and three anonymous reviewers for providing insightful comments and suggestions. During this study, authors were supported by the ARM program under Grant DE-A102-97ER62341, Dr. Dong was also supported by NASA CERES project under Contract NAG-1-2250, and Dr. Mace was also supported by NASA EOS validation project under Contract NAG-5-6458.

APPENDIX

New Cloud Parameterization

To retrieve the microphysical and radiative properties

of single-layer and overcast low-level stratus clouds, D97 used a delta–2-stream radiative transfer model in conjunction with ground-based measurements. The retrieval scheme is based on an iterative approach that varies r_e in the radiative transfer calculations until the model-calculated solar transmission matches the measured value. The retrieved cloud properties include the layer-mean cloud-droplet effective radius (r_e) and number concentration (N), broadband shortwave optical depth (τ), and albedos at the top of cloud and atmosphere (R_{cldy}, R_{TOA}) with the derived R_{sfc}. D98 parameterized the retrieved r_e and radiative properties as a function of the cloud LWP, the effective solar transmission (γ), and cosine of the solar zenith angle (μ_0). The retrieved and parameterized cloud microphysical properties have been validated by aircraft in situ measurements in the midlatitudes (Dong et al. 1998, 2002) and in the Arctic region (Dong et al. 2001).

The method to develop the new parameterization is the same as that in D98; at first we retrieve r_e using the D97 technique with the inputs of surface measurements, such as cloud LWP, ΔZ, γ, and R_{sfc}, and then we parameterize r_e as a polynomial function of cloud LWP, γ, μ_0, and R_{sfc}. The D98 parameterization is primarily developed for low R_{sfc} where single-layer, liquid-phase, and daytime cloud conditions exist. The new parameterization, reported here for the first time, is the same as that described by D98 except the impact of R_{sfc} is included. To demonstrate the impact of R_{sfc} on cloud albedo and transmission, Fig. A1 is plotted using a two-stream discrete-ordinate method (Liou 1974). The cloud albedo and transmission only depend on τ for $R_{\text{sfc}} = 0$, but they monotonically increase with increased R_{sfc}. The dependence of cloud albedo and transmission on τ becomes smaller with increased R_{sfc}. Therefore, cloud albedo and transmission depend on both τ and R_{sfc} for conservative scattering, as shown in Fig. A1. However, if clouds absorb appreciably, the influence of R_{sfc} on cloud albedo would depend on the amount of cloud absorption and τ. The effective solar transmission (γ), which relies on the measured total downward solar flux at the surface, also increases with increased R_{sfc} due to the multiple reflections of solar radiation between the cloud layer and the highly reflective surface.

To develop the new parameterization, we use 13 cases (~91 h of data) with the range of R_{sfc} from 0.1 to 0.9 selected from the present study period at the ARM NSA site. The retrieved values of r_e from the D97 method are parameterized as a polynomial function of cloud LWP, γ, μ_0, and R_{sfc} as follows:

$$r_e = 2.49\text{LWP} + 10.25(1 - R_{\text{sfc}}^3)\gamma - 0.25\mu_0 + 20.28\text{LWP}\gamma(1 - R_{\text{sfc}}^3) - 3.14\text{LWP}\mu_0, \quad \text{(A1)}$$

where the units of LWP and r_e are 100 g m^{-2} and μm, respectively. Equation (A1) is similar to (9) of D98 except that R_{sfc} is included. Once r_e is known, N and τ can be estimated

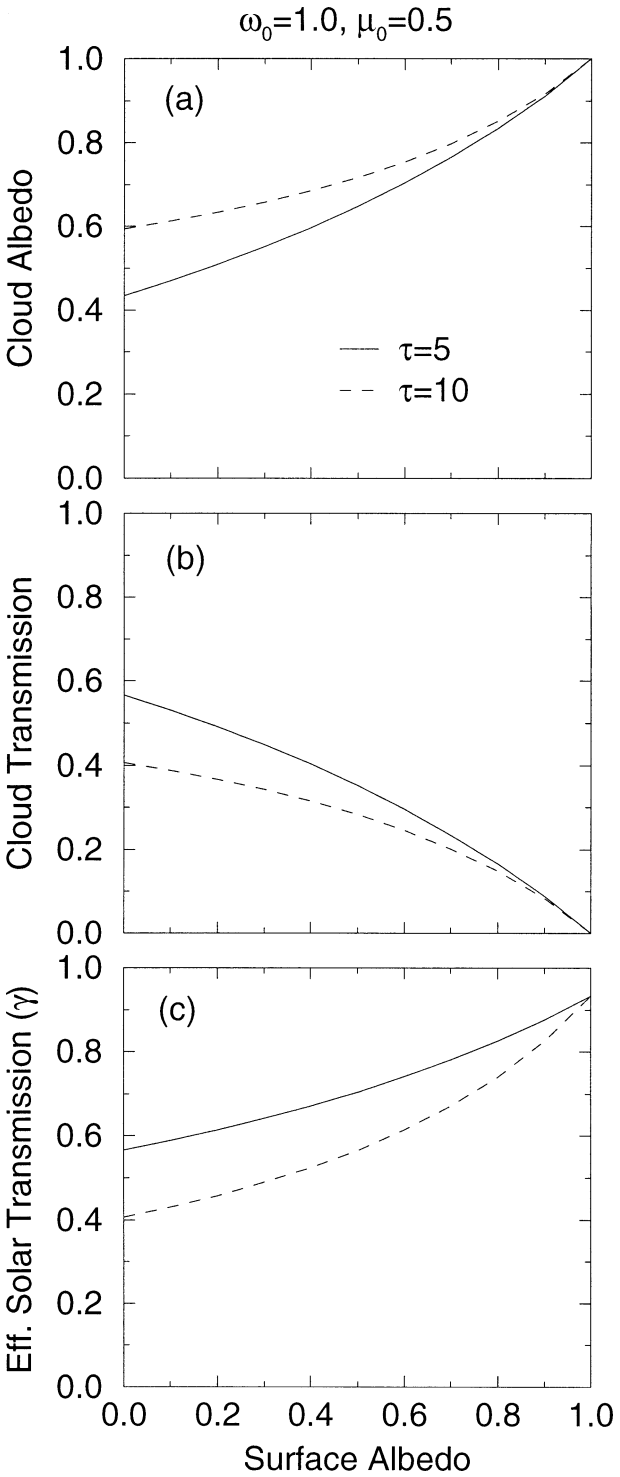

FIG. A1. (a) Cloud albedo and (b) transmission are calculated by a two-stream discrete-ordinate method to study the impact of surface albedo on cloud albedo and transmission. (c) The effective solar transmission (γ) is the total downward solar flux at the surface.

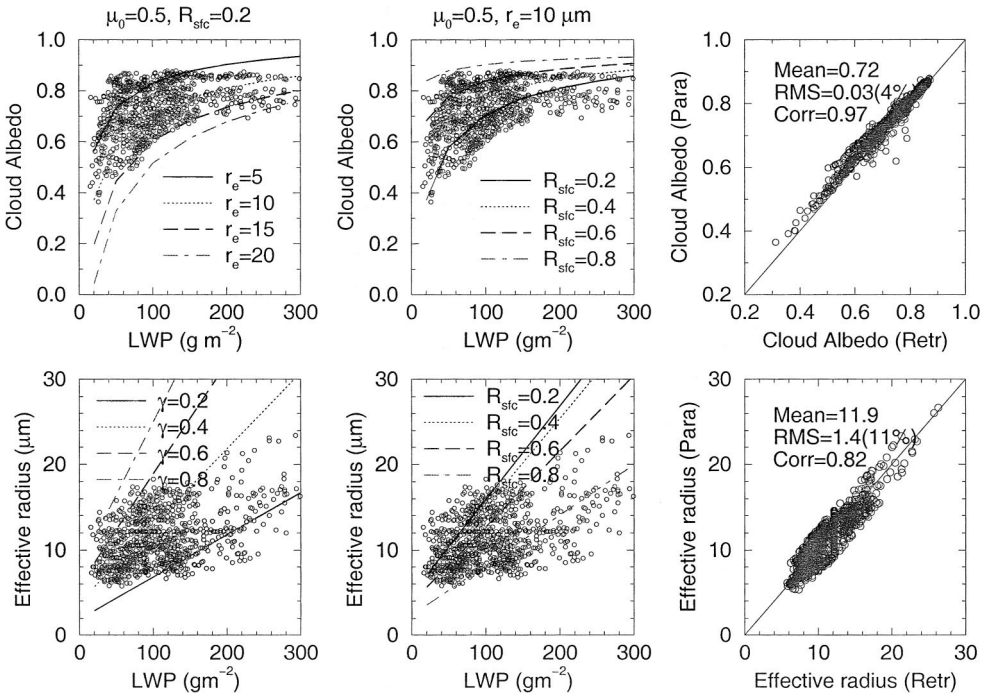

FIG. A2. The lines represent the calculated cloud-top albedo from (A6) and effective radius from (A1) with fixed μ_0 and $R_{\rm sfc}$ (or r_e and γ), and the circles represent the data (~91 h). The calculated cloud effective radius and albedo (parameterization) are also compared with the retrieved cloud properties (retrieval) in the right column.

$$N = \frac{3\mathrm{LWP}}{4\pi\rho_w r_e^3 \Delta Z}\exp(3\sigma_x^2), \quad \text{and} \tag{A2}$$

$$\tau = \frac{3\mathrm{LWP}}{2r_e\rho_w}. \tag{A3}$$

The logarithmic width σ_x is set to 0.38 (Miles et al. 2000), and ΔZ is cloud thickness derived from the difference of cloud-top and -base heights. Fixing σ_x in the scheme does not lead to significant errors in the retrieval values of r_e, while N changes by 15%–30% as σ_x varies from 0.2 to 0.5 (D97).

The D98 cloud albedo ($R_{\rm D98}$) and transmission ($T_{\rm D98}$) were calculated with the inputs of retrieved r_e and N, along with the measured cloud-base and -top heights using the same radiative transfer model as in the retrieval of r_e and N but with $R_{\rm sfc} = 0$. The resulting values for $R_{\rm D98}$ and $T_{\rm D98}$ are then fit with polynomial function of LWP, r_e, and μ_0:

$$\begin{aligned} R_{\rm D98} = {} & -0.089 - 0.089r_e - 0.19\mu_0 + 0.405\ln(\mathrm{LWP}) \\ & - 0.033\ln^2(\mathrm{LWP}) + 0.00045r_e^2 \\ & + 0.011\ln(\mathrm{LWP})r_e, \end{aligned} \tag{A4}$$

$$\begin{aligned} T_{\rm D98} = {} & 1.087 + 0.096r_e + 0.153\mu_0 - 0.418\ln(\mathrm{LWP}) \\ & + 0.034\ln^2(\mathrm{LWP}) - 0.0004r_e^2 \\ & - 0.012\ln(\mathrm{LWP})r_e, \end{aligned} \tag{A5}$$

where the units of LWP and r_e are g m^{-2} and μm, respectively. The $R_{\rm D98}$ and $T_{\rm D98}$ are nearly the same as the bulk cloud-top albedo $R_{\rm cldy}$ and measured γ over land and ocean for low $R_{\rm sfc}$, but not for high $R_{\rm sfc}$. The $R_{\rm cldy}$, a result found during the retrieval of r_e, has the following relationship with $R_{\rm D98}$, $T_{\rm D98}$, and $R_{\rm sfc}$ based on a total of 91 h of measurements and retrievals:

$$R_{\rm cldy} = R_{\rm D98} + R_{\rm sfc}T_{\rm D98}. \tag{A6}$$

The $R_{\rm cldy}$ in (A6) will equal $R_{\rm D98}$ if $R_{\rm sfc} = 0$. The bulk TOA albedo ($R_{\rm TOA}$), on average, is 82.6% of the $R_{\rm cldy}$ with only a 2% variation around the average value during the 91-h period. The rms errors in the parameterizations of r_e and $R_{\rm cldy}$ relative to the retrieved values are similar to those reported in D98, around 11% and 4% (Fig. A2), respectively.

To illustrate the importance of r_e and $R_{\rm sfc}$ to $R_{\rm cldy}$, Fig. A2 is produced from (A6) for a variety of cloud LWP, r_e and $R_{\rm sfc}$ with a specified μ_0. As Fig. A2 demonstrates, for fixed LWP, $R_{\rm cldy}$ has a significant dependence on both r_e and $R_{\rm sfc}$. The quantitative dependence of r_e on cloud LWP, γ, and $R_{\rm sfc}$ is also illustrated in Fig. A2 where r_e exhibits a strong positive correlation with γ for a given $R_{\rm sfc}$ and a negative correlation with $R_{\rm sfc}$ for a fixed γ. Most of data points (circles) fall within the lower and upper limits of calculations (lines) from the new parameterizations (A1, A6) as shown in Fig. A2.

REFERENCES

Barrie, L. A., 1986: Arctic air pollution: An overview of current knowledge. *Atmos. Environ.,* **20,** 643–663.

Bigg, E. K., 1980: Comparison of aerosol at four baseline atmospheric monitoring stations. *J. Appl. Meteor.,* **19,** 521–533.

Chakrapani, V., D. A. Spangenberg, D. R. Doelling, P. Minnis, Q. Z. Trepte, and R. F. Arduini, 2001: Improvements in AVHRR daytime cloud detection over the ARM NSA site. *Proc. 11th ARM Science Team Meeting,* Atlanta, GA, Dept. of Energy. [Available online at http://www.arm.gov/docs/documents/technical/conf_0103/author.html.]

Curry, J. A., and E. E. Ebert, 1992: Annual cycle of radiation fluxes over the Arctic Ocean: Sensitivity to cloud optical properties. *J. Climate,* **5,** 1276–1280.

——, W. B. Rossow, D. Randall, and J. L. Schramm, 1996: Overview of Arctic cloud and radiation characteristics. *J. Climate,* **9,** 1731–1764.

——, and Coauthors, 2000: FIRE Arctic Clouds Experiment. *Bull. Amer. Meteor. Soc.,* **81,** 5–29.

——, J. L. Schramm, D. K. Perovich, and J. O. Pinto, 2001: Applications of SHEBA/FIRE data to evaluation of snow/ice albedo parameterizations. *J. Geophys. Res.,* **106,** 15 345–15 355.

Dong, X., T. P. Ackerman, E. E. Clothiaux, P. Pilewskie, and Y. Han, 1997: Microphysical and radiative properties of stratiform clouds deduced from ground-based measurements. *J. Geophys. Res.,* **102,** 23 829–23 843.

——, ——, and ——, 1998: Parameterizations of microphysical and shortwave radiative properties of boundary layer stratus from ground-based measurements. *J. Geophys. Res.,* **103,** 31 681–31 693.

——, P. Minnis, T. P. Ackerman, E. E. Clothiaux, G. G. Mace, C. N. Long, and J. C. Liljegren, 2000: A 25-month database of stratus cloud properties generated from ground-based measurements at the ARM SGP site. *J. Geophys. Res.,* **105,** 4529–4538.

——, G. G. Mace, P. Minnis, and D. F. Young, 2001: Arctic stratus cloud properties and their effect on the surface radiation budget: Selected cases from FIRE ACE. *J. Geophys. Res.,* **106,** 15 297–15 312.

——, P. Minnis, G. G. Mace, W. L. Smith Jr., M. Poellot, R. T. Marchand, and R. P. Rapp, 2002: Comparison of stratus cloud properties deduced from surface, GOES, and aircraft data during the March 2000 ARM cloud IOP. *J. Atmos. Sci.,* **59,** 3265–3284.

Garrett, T. J., L. F. Radke, and P. V. Hobbs, 2002: Aerosol effects on cloud emissivity and surface longwave heating in the Arctic. *J. Atmos. Sci.,* **59,** 769–778.

Gates, W. L., 1992: AMIP: The Atmospheric Model Intercomparison Project. *Bull. Amer. Meteor. Soc.,* **73,** 1962–1970.

Harris, J. M., and J. D. W. Kahl, 1994: Analysis of 10-day isentropic flow patterns for Barrow, Alaska: 1985–1992. *J. Geophys. Res.,* **99,** 25 845–25 855.

Harrison, E. F., P. Minnis, B. R. Barkstrom, V. Ramanathan, R. D. Cess, and G. G. Gibson, 1990: Seasonal variation of cloud radiative forcing derived from the Earth Radiation Budget Experiment. *J. Geophys. Res.,* **95,** 18 687–18 703.

Hartmann, D. L., M. E. Ockert-Bell, and M. L. Michelsen, 1992: The effect of cloud type on earth's energy balance: Global analysis. *J. Climate,* **5,** 1281–1304.

Herman, G. F., and R. Goody, 1976: Formation and persistence of summertime Arctic stratus clouds. *J. Atmos. Sci.,* **33,** 1537–1553.

——, and J. A. Curry, 1984: Observational and theoretical studies of solar radiation in Arctic stratus clouds. *J. Climate Appl. Meteor.,* **23,** 5–24.

Hobbs, P. V., and A. L. Rangno, 1998: Microstructures of low and middle-level clouds over the Beaufort Sea. *Quart. J. Roy. Meteor. Soc.,* **124,** 2035–2071.

——, ——, M. D. Shupe, and T. Uttal, 2001: Airborne studies of cloud structures over the Arctic Ocean and comparisons with retrievals from ship-based remote sensing instruments. *J. Geophys. Res.,* **106,** 15 029–15 044.

Intrieri, J. M., C. W. Fairall, M. D. Shupe, P. O. G. Persson, E. L. Andreas, P. S. Guest, and R. E. Moritz, 2002a: An annual cycle of Arctic surface cloud forcing at SHEBA. *J. Geophys. Res.,* **107** (C10), 8039, doi:10.1029/2000JC000439.

——, M. D. Shupe, T. Uttal, and B. J. McCarty, 2002b: An annual cycle of Arctic cloud characteristics observed by radar and lidar at SHEBA. *J. Geophys. Res.,* **107** (C10), 8030, doi:10.1029/2000JC000423.

Kato, S., T. P. Ackerman, E. E. Clothiaux, J. H. Mather, G. G. Mace, M. L. Wesely, F. Murcray, and J. Michalsky, 1997: Uncertainties in modeled and measured clear-sky surface shortwave irradiance. *J. Geophys. Res.,* **102,** 25 881–25 898.

Krueger, S. K., 1988: Numerical simulation of tropical cumulus clouds and their interaction with the subcloud layer. *J. Atmos. Sci.,* **45,** 2221–2250.

Lawson, R. P., B. A. Baker, C. G. Schmitt, and T. L. Jensen, 2001: An overview of microphysical properties and Arctic clouds observed in May and July 1998 during FIRE ACE. *J. Geophys. Res.,* **106,** 14 989–15 014.

Leontyeva, E., and K. Stamnes, 1994: Estimates of cloud optical thickness from ground-based measurements of incoming solar radiation in the Arctic. *J. Climate,* **7,** 566–578.

Liljegren, J. C., E. E. Clothiaux, G. G. Mace, S. Kato, and X. Dong, 2001: A new retrieval for cloud liquid water path using a ground-based microwave radiometer and measurements of cloud temperature. *J. Geophys. Res.,* **106,** 14 485–14 500.

Liou, K. N., 1974: Analytic two-stream and four-stream solutions for radiative transfer. *J. Atmos. Sci.,* **31,** 1473–1475.

Long, C. N., and T. P. Ackerman, 2000: Identification of clear skies from broadband pyranometer measurements and calculation of downwelling shortwave cloud effects. *J. Geophys. Res.,* **105,** 15 609–15 626.

Mace, G. G., and K. Sassen, 2000: A constrained algorithm for retrieval of stratocumulus cloud properties using solar radiation, microwave radiometer, and millimeter cloud radar data. *J. Geophys. Res.,* **105,** 29 099–29 108.

Maslanik, J. A., J. Key, C. W. Fowler, T. Nguyen, and X. Wang, 2001: Spatial and temporal variability of satellite-derived cloud and surface characteristics during FIRE-ACE. *J. Geophys. Res.,* **106,** 15 223–15 249.

Miles, N. L., J. Verlinde, and E. E. Clothiaux, 2000: Cloud-droplet size distributions in low-level stratiform clouds. *J. Atmos. Sci.,* **57,** 295–311.

Minnis, P., and Coauthors, 2001: Cloud coverage and height during FIRE ACE derived from AVHRR data. *J. Geophys. Res.,* **106,** 15 215–15 232.

Mitchell, J. F. B., and W. J. Ingram, 1992: Carbon dioxide and climate: Mechanisms of changes in cloud. *J. Climate,* **5,** 5–21.

Moran, K. P., B. E. Martner, M. J. Post, R. A. Kropfli, D. C. Welsh, and K. B. Widener, 1998: An unattended cloud-profiling radar for use in climate research. *Bull. Amer. Meteor. Soc.,* **79,** 443–455.

Paluch, I. R., and D. H. Lenschow, 1991: Stratiform cloud formation in the marine boundary layer. *J. Atmos. Sci.,* **48,** 2141–2158.

Perovich, D. K., and Coauthors, 1999: Year on ice gives climate insights. *Eos, Trans. Amer. Geophys. Union,* **80,** 481–486.

Pinto, J. O., J. A. Curry, and J. M. Intrieri, 2001: Cloud–aerosol interactions during the autumn over Beaufort Sea. *J. Geophys. Res.,* **106,** 15 077–15 097.

Ramanathan, V., R. D. Cess, E. F. Harrison, P. Minnis, B. R. Barkstrom, E. Ahmad, and D. Hartmann, 1989: Cloud-radiative forcing and climate: Results from the Earth Radiation Budget Experiment. *Science,* **243,** 57–63.

Randall, D., K.-M. Xu, R. J. C. Somerville, and S. Iacobellis, 1996: Single-column models and cloud ensemble models as links between observations and climate models. *J. Climate,* **9,** 1683–1697.

——, and Coauthors, 1998: Status of and outlook for large-scale modeling of atmospheric–ice–ocean interactions in the Arctic. *Bull. Amer. Meteor. Soc.,* **78,** 197–219.

Stamnes, K., R. G. Ellingson, J. A. Curry, J. E. Walsh, and B. D. Zak, 1999: Review of science issues, deployment strategy, and status for the ARM North Slope of Alaska–Adjacent Arctic Ocean climate research site. *J. Climate,* **12,** 46–63.

Stokes, G. M., and S. E. Schwartz, 1994: The Atmospheric Radiation Measurement (ARM) program: Programmatic background and

design of the cloud and radiation testbed. *Bull. Amer. Meteor. Soc.,* **8,** 1251–1256.
Stone, R. S., 1997: Variations in western arctic temperature in response to cloud radiative and synoptic-scale influence. *J. Geophys. Res.,* **102,** 21 769–21 776.
Tao, X., J. E. Walsh, and W. L. Chapman, 1996: An assessment of global climate simulations of Arctic air temperatures. *J. Climate,* **9,** 1060–1076.
Tsay, S.-C., and K. Jayaweera, 1984: Physical characteristics of Arctic stratus clouds. *J. Climate Appl. Meteor.,* **23,** 584–596.
Westwater, E. R., Y. Han, M. D. Shupe, and S. Y. Matrosov, 2001: Analysis of integrated cloud liquid and precipitable water vapor retrievals from microwave radiometers during SHEBA. *J. Geophys. Res.,* **106,** 32 019–32 030.
Wetherald, R. T., and S. Manabe, 1988: Cloud feedback processes in general circulation model. *J. Atmos. Sci.,* **45,** 1397–1415.